Journal of Physics and Chemistry of Solids 72 (2011) 891–898

Contents lists available at ScienceDirect

Journal of Physics and Chemistry of Solids

journal homepage: www.elsevier.com/locate/jpcs

Superparamagnetic-like behavior and spin–orbit coupling in (Co,Zn)$RE_4W_3O_{16}$ tungstates (RE=Nd, Sm, Eu, Gd, Dy and Ho)

P. Urbanowicz [a], E. Tomaszewicz [b], T. Groń [a,*], H. Duda [a], A.W. Pacyna [c], T. Mydlarz [d], H. Fuks [e], S.M. Kaczmarek [e], J. Krok-Kowalski [a]

[a] University of Silesia, Institute of Physics, ul. Uniwersytecka 4, 40-007 Katowice, Poland
[b] West Pomeranian University of Technology, Department of Inorganic and Analytical Chemistry, Al. Piastów 42, 71-065 Szczecin, Poland
[c] The Henryk Niewodniczański Institute of Nuclear Physics, Polish Academy of Sciences, ul. Radzikowskiego 152, 31-342 Kraków, Poland
[d] International Laboratory of High Magnetic Fields and Low Temperatures, ul. Gajowicka 95, 53-529 Wrocław, Poland
[e] West Pomeranian University of Technology, Institute of Physics, Al. Piastów 17, 70-310 Szczecin, Poland

ARTICLE INFO

Article history:
Received 7 October 2010
Received in revised form
18 March 2011
Accepted 20 April 2011
Available online 4 May 2011

Keywords:
A. Oxides
B. Chemical synthesis
D. Magnetic properties

ABSTRACT

Magnetic susceptibility measurements carried out on (Co,Zn)$RE_4W_3O_{16}$ compounds revealed a disordered state of magnetic moments above 4.2 K for all compounds under study, and a weak response to magnetic field and temperature for $ZnSm_4W_3O_{16}$ and $ZnEu_4W_3O_{16}$ samples. The temperature independent component of magnetic susceptibility has a negative value for $ZnGd_4W_3O_{16}$ and a positive one for the rest of the tungstates, indicating a domination of van Vleck contribution. The magnetization isotherms of majority of the tungstates under study revealed both spontaneous magnetic moments and hysteresis characteristic for the superparamagnetic-like behavior with blocking temperature $T_B \sim 30$ K, except for $ZnEu_4W_3O_{16}$. Fitting procedure of the Landé factor revealed that the stronger the orbital contribution, the weaker the superparamagnetic effect, namely for $ZnRE_4W_3O_{16}$. In case of $CoRE_4W_3O_{16}$ a significant participation of the Co^{2+} moment in the spontaneous magnetization was observed.

1. Introduction

Nowadays, white light emitting diodes (WLEDs) are important class of lighting devices and, because of their great advantages (low energy consumption, long lifetime, high stability, and being environmental-friendly); they can replace traditional light sources such as incandescent and fluorescent lamps. WLEDs, as white light sources, are already commonly used to illuminate architecture, as medical lighting and backlights for portable electronics. Presently used method of WLEDs production is to combine red, green and blue phosphors with near UV InGaN-based LEDs [1,2].

Some promising materials to use in WLEDs are, *e.g.*, doped and undoped double rare-earth tungstates, molybdates and molybdato-tungstates such as: $Sr_9RE_{2-x}Eu_xW_4O_{24}$ (RE=Y, Gd) [3], $LiY_{1-x}Eu_x(MoO_4)_2$ [4], $NaM(WO_4)_{2-x}(MoO_4)_x:Eu^{3+}$ (M=Gd, Y, Bi) [1], $KEu(WO_4)_{2-x}(MoO_4)_x$ [5] and $LiEu(WO_4)_{2-x}(MoO_4)_x$ [6]. These host materials with various crystal structures have got excellent luminescence properties, and high thermal and chemical stability.

In recent years, more and more interest has been put into synthesis of new phosphors with interesting optical properties and containing both *d*- and *f*-electron metal ions [7–11]. The introduction of *d*-electron metal ions may give luminescent materials having very interesting magnetic and electrical properties.

It is well known that zinc tungstate ($ZnWO_4$, the wolframite type structure, S.G. *P2/c* [12]) reacts in the solid-state with some rare-earth metal tungstates (RE_2WO_6) to give a family of isostructural compounds with a general formula $ZnRE_4W_3O_{16}$ (RE=Y, Nd, Sm, Eu, Gd, Dy and Ho) [13]. The $ZnRE_4W_3O_{16}$ compounds crystallize in the orthorhombic system and they melt incongruently or decompose in the solid state above 1523 K [13]. The photoluminescence studies have been carried out for $ZnEu_4W_3O_{16}$ and $ZnY_{4-x}Eu_xW_3O_{16}$ solid solutions (x=0.01, 0.05 and 0.10) [13]. The $ZnEu_4W_3O_{16}$ compound has a strong red emission under 394 nm, which is due to an electron transition of Eu^{3+} ion ($^7F_0 \rightarrow {}^5L_6$) [14]. The emission of this compound shows very good Commission Internationale de l'Eclairage (CIE) chromaticity coordinates (x=0.66, y=0.33) near to the National Television Standard Committee (NTSC) standard values (x=0.67, y=0.33) [14]. For $ZnY_{4-x}Eu_xW_3O_{16}$ solid solutions, the emission from higher ^5D_J states of Eu^{3+} ion was additionally observed. With decrease in Eu^{3+} concentration in the $ZnY_{4-x}Eu_xW_3O_{16}$

* Corresponding author.
E-mail address: Tadeusz.Gron@us.edu.pl (T. Groń).

0022-3697/$ - see front matter © 2011 Elsevier Ltd. All rights reserved.
doi:10.1016/j.jpcs.2011.04.012

solid solutions, the color was shifted, and $ZnY_{3.99}Eu_{0.01}W_3O_{16}$ had to be a white-emitting phosphor [14].

Our earlier studies concerning reactivity in the solid state between $CoWO_4$ and RE_2WO_6 (RE=Sm–Gd) have shown existence of two families of new compounds, i.e., $Co_2RE_2W_3O_{14}$ and $CoRE_4W_3O_{16}$ [15]. These compounds crystallize in the orthorhombic system, and they melt above 1423 K [15]. It was also found that $CoRE_4W_3O_{16}$ compounds are isostructural with $ZnRE_4W_3O_{16}$ phases [15]. Electron paramagnetic resonance (EPR) studies of $Co_2Gd_2W_3O_{14}$ and $CoGd_4W_3O_{16}$ indicated an antiferromagnetic interaction of Gd^{3+}-Gd^{3+} spins with $\theta=-12$ K and $\theta=-11.7$ K, respectively [16]. IR spectra of (Co,Zn)$RE_4W_3O_{16}$ compounds suggest that their anion lattice is built of isolated WO_5 trigonal bipyramids or joint WO_6 octahedra forming $[(W_2O_9)^{6-}]\infty$-structural elements [13,15].

The main purpose of the present work is an attempt to study and summarize magnetic properties of powder (Co,Zn)$RE_4W_3O_{16}$ samples, where RE=Nd, Sm, Eu, Gd, Dy and Ho. EPR and the Brillouin fit of the Landé factor were used in order to understand electron transitions in (Co,Zn)$RE_4W_3O_{16}$. Knowledge of these phenomena in the above mentioned compounds is important from the viewpoint of their WLEDs application.

2. Experimental

2.1. Sample preparation

Polycrystalline samples of $ZnRE_4W_3O_{16}$ and $CoRE_4W_3O_{16}$ were prepared by conventional ceramic method. $ZnWO_4$, $CoWO_4$ and RE_2WO_6 (RE=Nd, Sm, Eu, Gd, Dy and Ho) were used as the starting materials. Stoichiometric amounts of starting reactants were mixed in an agate mortar and heated in air, under conditions described previously [13,15]. Phase purity of the products obtained was confirmed by powder XRD method using a DRON-3 diffractometer operating at 40 kV/20 mA and CoK_α radiation ($\lambda=0.179021$ nm).

2.2. Magnetic and electrical measurements

Dynamic (ac) magnetic susceptibility was measured using a Lake Shore 7225 ac susceptometer in the temperature range 4.2–280 K and at internal oscillating magnetic field $H_{ac}=1$ Oe with internal frequency $f=125$ Hz. Static (dc) magnetic susceptibility and magnetization isotherm measurements were performed using a Faraday type Cahn RG automatic electrobalance up to 300 K and a vibrating sample magnetometer with a step motor in applied external fields up to 14 T, respectively. Both dc and ac susceptibilities as well as the magnetization isotherms were measured in the zero-field-cooled (ZFC) mode. A diamagnetic contribution has been taken into account [17], and a Curie–Weiss law was fitted by adding a temperature independent contribution of magnetic susceptibility (χ_0) [18]. The fitted reciprocal magnetic susceptibility $1/(\chi_\sigma-\chi_0)$ is marked in red. This dependence is approximated by the red straight line $(T-\theta)/C_\sigma$, which intersects the temperature axis at $T=\theta$, and its inclination equals to $1/C_\sigma$.

The electrical measurements were made with the aid of four-probe dc method using a semi-automatic bridge with an input impedance of 1.5 TΩ, and showed that all tungstates under study are insulators. For electrical measurements, the powder samples were compacted in disk form (10 mm in diameter and 1–2 mm thick) using pressure of 1.5 GPa, and next they were sintered at 473 K for 2 h.

2.3. EPR measurements

EPR measurements were performed with a conventional X-band Bruker ELEXSYS E500 CW spectrometer operating at 9.5 GHz with 100 kHz magnetic field modulation. Temperature dependence of the EPR spectra was registered in the 4.5–220 K temperature range using an Oxford flow cryostat to control it.

3. Results and discussion

3.1. Magnetic properties

The results of magnetic susceptibility measurements of $ZnRE_4W_3O_{16}$ and $CoRE_4W_3O_{16}$ tungstates are depicted in Table 1 and in Figs. 1–7. Majority of the tungstates under study show both small and negative values of paramagnetic Curie–Weiss temperature and positive values of temperature independent contribution of magnetic susceptibility. It may indicate a residual magnetic interaction without any cluster interactions below 4.2 K from one side and temperature independent contributions of the orbital and Landau diamagnetism, Pauli and Van Vleck paramagnetism as well as others from the other side, as they cannot be separated. Because the tungstates under study are insulators the Landau and Pauli contributions can be neglected. Looking more precisely, $ZnNd_4W_3O_{16}$ and $CoEu_4W_3O_{16}$ compounds in Figs. 1 and 6 reveal low values of magnetic susceptibility, $\chi_\sigma\sim10^{-4}$ cm^3/g. $ZnEu_4W_3O_{16}$ (Fig. 2) has only $\chi_\sigma\sim10^{-5}$ cm^3/g and a weak temperature dependence of the susceptibility without a Curie–Weiss region. Finally, static

Table 1
Magnetic parameters of (Co,Zn)$RE_4W_3O_{16}$ (where RE=Nd, Sm, Eu, Gd, Dy and Ho): C_σ is the Curie constant, μ_{eff} is the effective magnetic moment, θ is the Curie–Weiss temperature, χ_0 is the temperature independent contribution of magnetic susceptibility, σ is the experimental magnetization at 4.2 K and at 14 T, J is the effective angular momentum explained in detail in the text, g is the Landé factor of the Co^{2+} and the RE-elements, σ_0 is the magnetization at the highest value of H/T, g_{fit} is the Landé factor estimated from the Brillouin fitting procedure and R^2 is the agreement index.

Compound	Measurements					Atomic data		Brillouin fit		
	C_σ (K cm^3/g)	μ_{eff} (μ_B/f.u.)	θ (K)	χ_0 (cm^3/g)	σ (μ_B/f.u.)	J	g	σ_0 (μ_B/f.u.)	g_{fit}	R^2 (%)
$ZnNd_4W_3O_{16}$	2.907×10^{-3}	5.81	−5.5	7.716×10^{-6}	3.67	9/2	8/11	4.03	0.55	99.87
$ZnSm_4W_3O_{16}$	–	–	–	–	–	5/2	2/7	–	–	–
$ZnEu_4W_3O_{16}$	–	–	–	–	0.49	0	–	–	–	–
$ZnGd_4W_3O_{16}$	2.000×10^{-2}	15.51	0.1	-1.978×10^{-8}	26.28	7/2	2	26.80	1.38	99.95
$ZnDy_4W_3O_{16}$	3.369×10^{-2}	20.26	−1.7	1.346×10^{-5}	13.45	15/2	4/3	13.26	1.03	99.26
$ZnHo_4W_3O_{16}$	3.04×10^{-2}	19.31	−1.4	1.923×10^{-5}	19.07	8	5/4	18.56	1.03	98.36
$CoSm_4W_3O_{16}$	–	–	–	–	1.34	4	4/3 (Co^{2+}) 2/7 (Sm^{3+})	1.38	0.66	99.16
$CoEu_4W_3O_{16}$	$6.715\cdot10^{-3}$	8.90	−113	2.288×10^{-6}	3.01	3/2	4/3 (Co^{2+})	3.03	1.20	99.38
$CoGd_4W_3O_{16}$	$2.194\cdot10^{-2}$	16.21	-0.9	9.523×10^{-7}	15.45	5	4/3 (Co^{2+}) 2 (Gd^{3+})	15.95	0.81	99.94

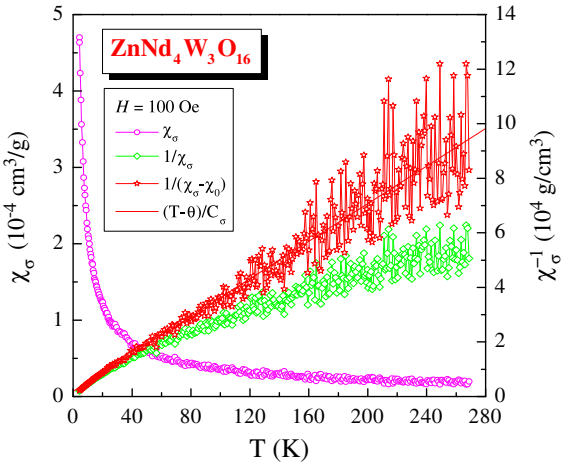

Fig. 1. Static susceptibility χ_σ, $1/\chi_\sigma$ and $1/(\chi_\sigma-\chi_0)$ vs. temperature T for $ZnNd_4W_3O_{16}$ recorded at $H=100$ Oe.

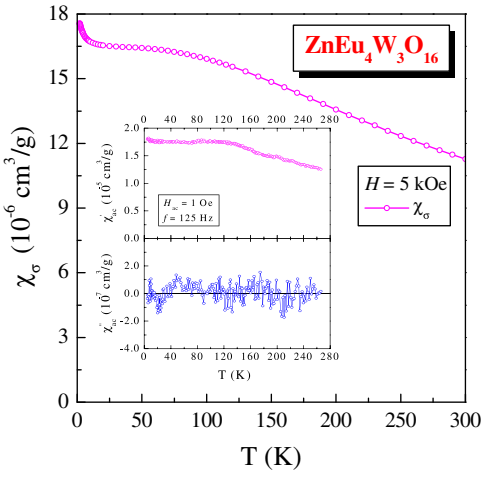

Fig. 2. Static susceptibility χ_σ vs. temperature T for $ZnEu_4W_3O_{16}$ recorded at $H=5$ kOe. Insert: In phase $\chi'_{ac}(T)$ and out of phase $\chi''_{ac}(T)$ components of dynamic susceptibility vs. temperature T recorded at internal oscillating magnetic field $H_{ac}=1$ Oe with internal frequency $f=125$ Hz.

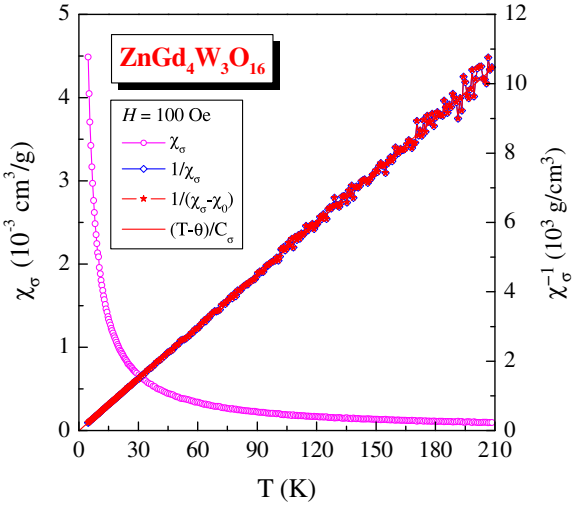

Fig. 3. Static susceptibility χ_σ and $1/\chi_\sigma$ vs. temperature T for $ZnGd_4W_3O_{16}$ recorded at $H=100$ Oe.

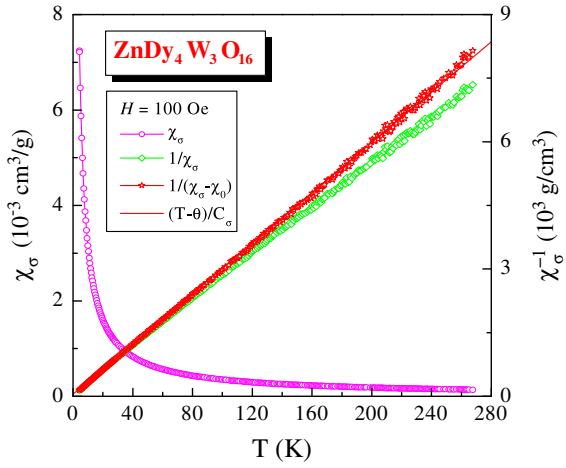

Fig. 4. Static susceptibility χ_σ, $1/\chi_\sigma$ and $1/(\chi_\sigma-\chi_0)$ vs. temperature T for $ZnDy_4W_3O_{16}$ recorded at $H=100$ Oe.

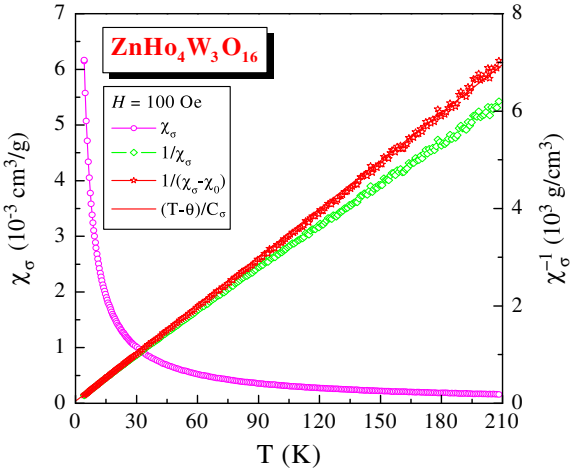

Fig. 5. Static susceptibility χ_σ, $1/\chi_\sigma$ and $1/(\chi_\sigma-\chi_0)$ vs. temperature T for $ZnHo_4W_3O_{16}$ recorded at $H=100$ Oe.

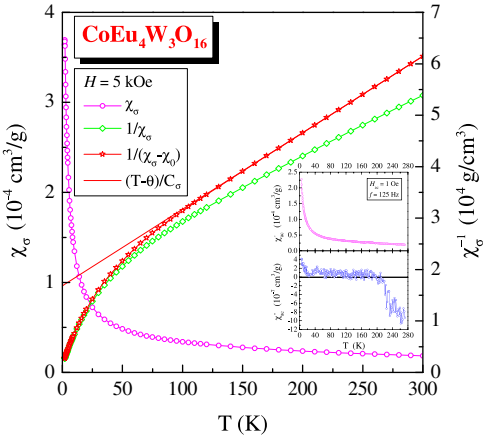

Fig. 6. Static susceptibility χ_σ, $1/\chi_\sigma$ and $1/(\chi_\sigma-\chi_0)$ vs. temperature T for $CoEu_4W_3O_{16}$ recorded at $H=5$ kOe. Inset: in phase $\chi'_{ac}(T)$ and out of phase $\chi''_{ac}(T)$ components of dynamic susceptibility vs. temperature T recorded at internal oscillating magnetic field $H_{ac}=1$ Oe with internal frequency $f=125$ Hz.

magnetic susceptibility of $ZnSm_4W_3O_{16}$ and $CoSm_4W_3O_{16}$ tungstates was almost impossible to measure because of small dc signal comparable to the sensitiveness limit of the apparatus. The temperature dependence of the in-phase $\chi'_{ac}(T)$ (real part)

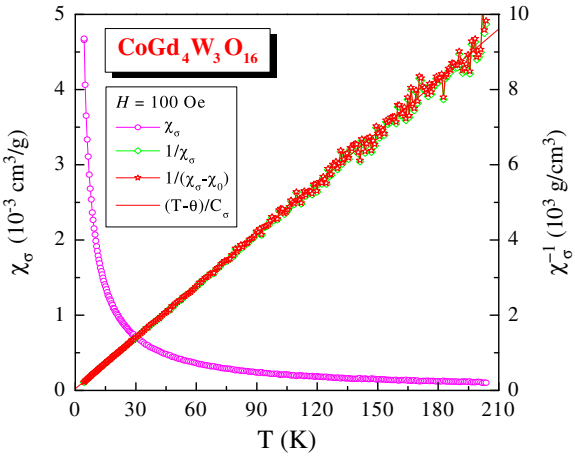

Fig. 7. Mass susceptibility χ_σ, $1/\chi_\sigma$ and $1/(\chi_\sigma-\chi_0)$ vs. temperature T for $CoGd_4W_3O_{16}$ recorded at $H=100$ Oe.

component of ac susceptibility of $ZnEu_4W_3O_{16}$ depicted in the insert of Fig. 2 coincides well with the dc measurement. A similar behavior was observed for $CoEu_4W_3O_{16}$ compound (see insert of Fig. 6). However, the out-of-phase $\chi''_{ac}(T)$ (imaginary part) component of ac susceptibility shows an absence of the energy losses for $ZnEu_4W_3O_{16}$ and reveals anomalies below 20 K and above 220 K for $CoEu_4W_3O_{16}$.

Effective magnetic moment of $ZnNd_4W_3O_{16}$, $ZnGd_4W_3O_{16}$, $ZnDy_4W_3O_{16}$ and $ZnHo_4W_3O_{16}$ tungstates (Figs. 1–5) is close to the theoretical one for the free rare-earth ion, given by the $g[J(J+1)]^{1/2}$ expression [17], while it is smaller for $CoEu_4W_3O_{16}$ and larger for $CoGd_4W_3O_{16}$ tungstates (Figs. 6 and 7), suggesting an influence of Co ions on the spontaneous magnetization. Effective magnetic moment has not been determined for $ZnSm_4W_3O_{16}$ and $ZnEu_4W_3O_{16}$ compounds because of the lack of the Curie–Weiss region. It may be connected with the fact that the narrower multiplet widths, comparable to kT, occur in the case of samarium and europium [19], so that not all the atoms are in their ground state [17]. Such levels above the ground state may not contribute to the magnetic susceptibility [20]. Similar behavior has been observed for Sm_2WO_6 and Eu_2WO_6 compounds [21].

$ZnGd_4W_3O_{16}$ tungstate (Fig. 3) requires a special attention because of small values of both positive paramagnetic Curie–Weiss temperature $\theta=0.1$ K and the negative temperature independent contribution of magnetic susceptibility $\chi_0=-1.978\cdot10^{-8}$ cm^3/g, indicating a lack and/or existence of only parasitic magnetic interactions from one side and a compensation of different temperature independent magnetic susceptibility contributions from the other one. By that reason, $ZnGd_4W_3O_{16}$ tungstate could serve as a paramagnetic standard. For comparison, $HgCo(CNS)_4$ compound, commonly accepted as a paramagnetic standard, has the following relevant parameters: $\theta=-1.86$ K and $\chi_0=0.427\times10^{-6}$ cm^3/g reported by Brown et al. [22] or $\theta=-0.32$ K and $\chi_0=0.484\times10^{-6}$ cm^3/g reported by Nelson and ter Haar [23].

The results of magnetic moment measurements of $ZnRE_4W_3O_{16}$ and $CoRE_4W_3O_{16}$ tungstates are shown in Table 1 and in Figs. 8–15. Magnetization isotherms, $\sigma(\mu_0H)$, of majority of the tungstates revealed both spontaneous magnetic moments and a hysteresis below 30 K. In an ideal paramagnet, there is no hysteresis in the field dependence of magnetization. It can appear in the superparamagnet for which the fluctuations of the magnetization vector among the easy directions of magnetization are blocked. In other words, the hysteresis both with zero coercivity and remanence is a consequence of the stable magnetization of a single domain particle, and temperature at which this occurs is called blocking temperature (T_B) [24]. As the studied tungstates

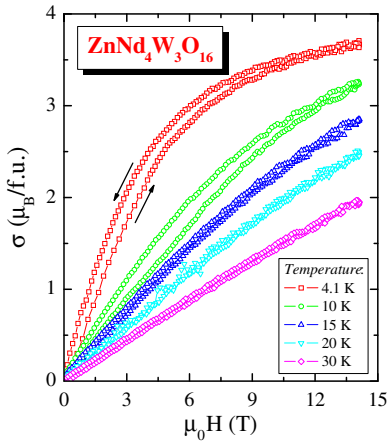

Fig. 8. Magnetization σ vs. magnetic field μ_0H for $ZnNd_4W_3O_{16}$ at 4.2, 10, 15, 20 and 30 K. A run of magnetic field is indicated by arrows.

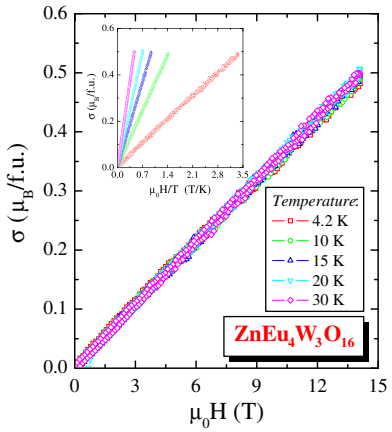

Fig. 9. Magnetization σ vs. magnetic field μ_0H for $ZnEu_4W_3O_{16}$ at 4.2, 10, 15, 20 and 30 K. Insert: magnetization σ as a function of μ_0H/T showing paramagnetic behavior.

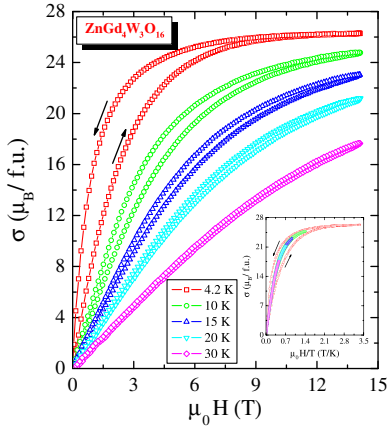

Fig. 10. Magnetization σ vs. magnetic field μ_0H for $ZnGd_4W_3O_{16}$ at 4.2, 10, 15, 20 and 30 K. A run of magnetic field is indicated by arrows. Insert: magnetization σ as a function of μ_0H/T showing superparamagnetic behavior.

are powders with particle sizes of the order of microns, they can be treated as the single-domain superparamagnetic particles with stable magnetization below T_B. In our case, $T_B\sim30$ K may be equivalently defined as a temperature at which the hysteresis loop disappears. An experimental feature characterizing superparamagnetism is a universal function of magnetization (σ) vs. magnetic field divided by temperature (μ_0H/T) [24]. This feature

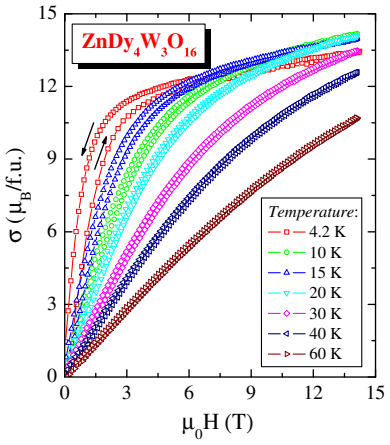

Fig. 11. Magnetization σ vs. magnetic field $\mu_0 H$ for $ZnDy_4W_3O_{16}$ at 4.2, 10, 15, 20, 30, 40 and 60 K. A run of magnetic field is indicated by arrows.

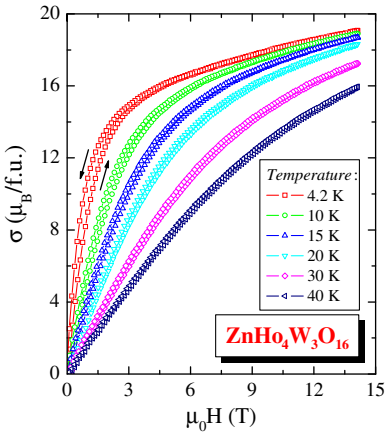

Fig. 12. Magnetization σ vs. magnetic field $\mu_0 H$ for $ZnHo_4W_3O_{16}$ at 4.2, 10, 15, 20, 30 and 40 K. A run of magnetic field is indicated by arrows.

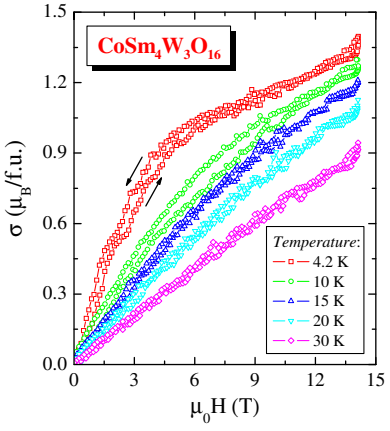

Fig. 13. Magnetization σ vs. magnetic field $\mu_0 H$ for $CoSm_4W_3O_{16}$ at 4.2, 10, 15, 20 and 30 K. A run of magnetic field is indicated by arrows.

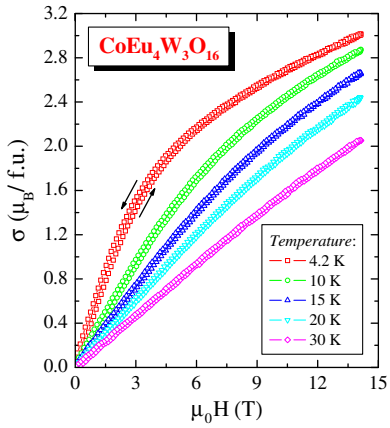

Fig. 14. Magnetization σ vs. magnetic field $\mu_0 H$ for $CoEu_4W_3O_{16}$ at 4.2, 10, 15, 20 and 30 K. A run of magnetic field is indicated by arrows.

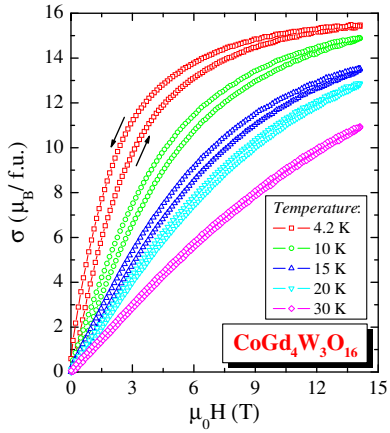

Fig. 15. Magnetization σ vs. magnetic field $\mu_0 H$ for $CoGd_4W_3O_{16}$ at 4.2, 10, 15, 20 and 30 K. A run of magnetic field is indicated by arrows.

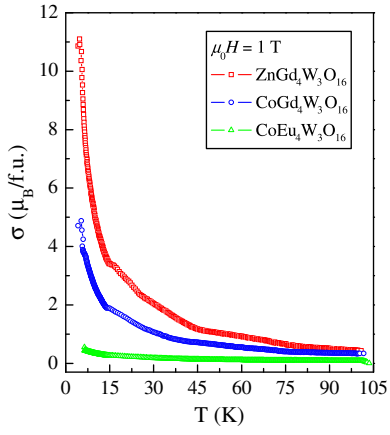

Fig. 16. Magnetization σ vs. temperature T at $\mu_0 H = 1$ T for $CoEu_4W_3O_{16}$, $CoGd_4W_3O_{16}$ and $ZnGd_4W_3O_{16}$.

is ideally obeyed for $ZnGd_4W_3O_{16}$ (inset of Fig. 10) and it is absent for $ZnEu_4W_3O_{16}$ (inset of Fig. 9). For the remaining tungstates, the magnetization curves $\sigma(\mu_0 H/T)$ usually deviate from the universal function. It may be connected with a significant orbital contribution to magnetic moment, discussed later.

Fig. 16 presents the temperature dependence of magnetization at magnetic field $\mu_0 H = 1$ T for $ZnGd_4W_3O_{16}$, $CoGd_4W_3O_{16}$ and $CoEu_4W_3O_{16}$ tungstates, which is characteristic for paramagnetic state. It has been independently confirmed by the EPR measurements [16]. The reduction of magnetic moment at 4.2 K and at 14 T from 26.3 μ_B/f.u. for $ZnGd_4W_3O_{16}$ (Fig. 10) to 15.5 μ_B/f.u. for $CoGd_4W_3O_{16}$ (Fig. 15) is anomaly large because these both tungstates are magnetically disordered. Their effective magnetic moments of 15.51 and 16.21 μ_B/f.u., estimated from the equation: $\mu_{eff} = 2.83\sqrt{MC_\sigma}$, where M is the molar mass and C_σ is the Curie constant taken from experiment (Table 1), are almost perfectly

close to the theoretical values of 15.87 and 16.34, respectively. They were calculated from the following equation: $p_{\text{eff}} = \sqrt{p_{\text{Co}}^2 + 4p_{\text{Gd}}^2}$, where $p = g\sqrt{J(J+1)}$ for a Gd^{3+} ion ($J=7/2$, $g=2$) with $4f^7$ and for a Co^{2+} ion ($S=3/2$, $g=2$) with $3d^7$. In the latter case, $S=3/2$ for Co^{2+} was taken from the EPR-experiment, because for the unprotected transition metal (TM) $3d$-shell, the crystal field perturbs the *JLS* coupling such that J and L are not good quantum numbers anymore—only S remains as such. It means that the Gd^{3+} and Co^{2+} ions exist in a sample and saturation magnetization in $CoGd_4W_3O_{16}$ larger than 26.3 μ_B/f.u. is expected in magnetic fields much stronger than 14 T. Therefore, the anomaly large reduction of magnetic moment at 14 T for $CoGd_4W_3O_{16}$ may suggest an antiparallel orientation of the Co^{2+} and Gd^{3+} moments in a molecule with the volume of 0.93687 nm^3 [15], which is induced by the uniaxial anisotropy [25]. Such molecules may form the single-domain ferrimagnetic nanoparticles, which exhibit only paramagnetic response. The main source of the anisotropy field is the spin–orbit coupling and the anisotropy distribution of the electron density. When the system involves magnetic moments with an easy magnetization axis, anisotropy energy reaches minimum. The value of anisotropy energy, K_a, defined as 1/8 of the area of the hysteresis cycle, irrespective of its shape [25], decreases with increase in temperature for $ZnGd_4W_3O_{16}$ and $CoGd_4W_3O_{16}$ tungstates (Fig. 17). Similar behavior for the remaining tungstates under study is seen in Figs. 8 and 11–14. Lower values of K_a for $CoGd_4W_3O_{16}$ in comparison with $ZnGd_4W_3O_{16}$ may result from the interactions between magnetic moments of Co^{2+} and Ga^{3+} ions in a particle, leading to the reduction of total magnetic moment experimentally observed. It is noteworthy that the presence of Co^{2+} ions strongly weakens the anisotropy and the values of K_a are comparable at the blocking temperature T_B for both above mentioned tungstates (see Fig. 17).

In conclusion, the magnetic measurements presented above have shown that the tungstates under study are paramagnets without any cluster interactions, even small. Some of them behave like superparamagnets below the blocking temperature of 30 K.

3.2. EPR spectra

The temperature evolution of the EPR spectra of $ZnGd_4W_3O_{16}$ and $CoGd_4W_3O_{16}$ tungstates are presented in Figs. 18 and 19, respectively. Their resonance linewidth ΔB and spin susceptibility, calculated as a double integration of the spectrum DI vs.

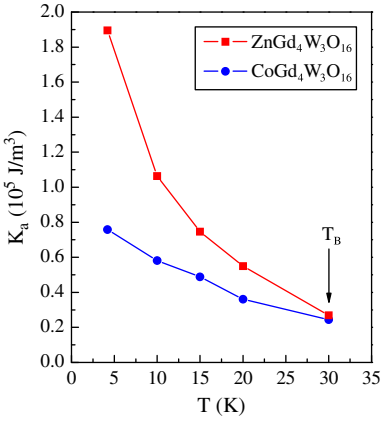

Fig. 17. Anisotropy energy K_a vs. temperature T for $CoGd_4W_3O_{16}$ and $ZnGd_4W_3O_{16}$ tungstates. T_B is the blocking temperature.

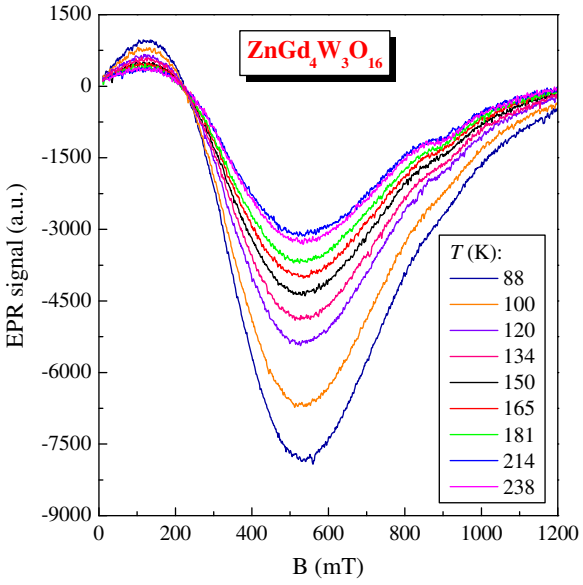

Fig. 18. EPR signals of $ZnGd_4W_3O_{16}$ measured at different temperatures.

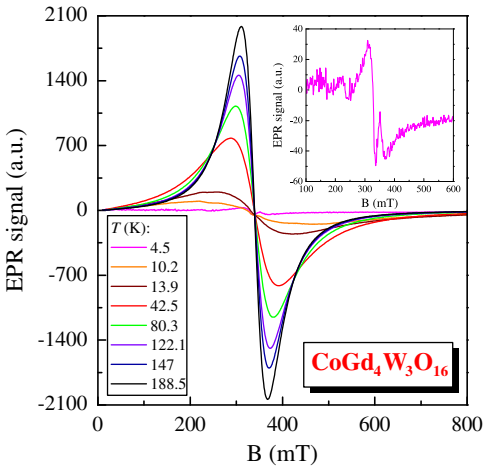

Fig. 19. EPR signals of $CoGd_4W_3O_{16}$ measured at different temperatures. Insert: the resonance curve at 4.5 K drawn to guide the eyes.

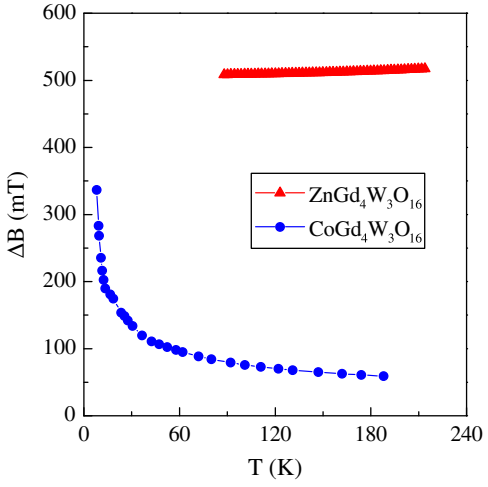

Fig. 20. Linewidth of the EPR signal ΔB vs. temperature T for $ZnGd_4W_3O_{16}$ and $CoGd_4W_3O_{16}$.

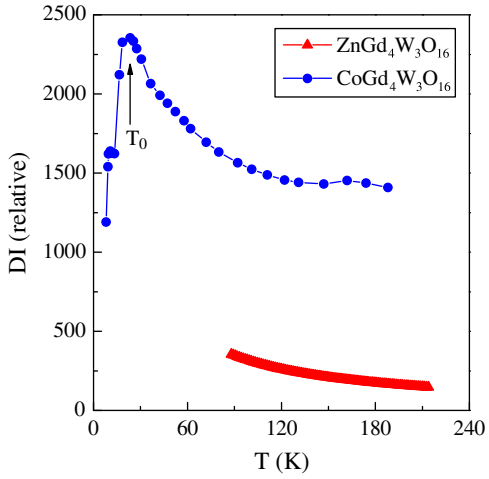

Fig. 21. EPR susceptibility as a double integration of the spectrum *DI* vs. temperature *T* for $ZnGd_4W_3O_{16}$ and $CoGd_4W_3O_{16}$. T_0 is the *DI* susceptibility characteristic temperature.

temperature *T*, are shown in Figs. 20 and 21, respectively. These dependences differ significantly for both compounds.

The EPR spectra of $ZnGd_4W_3O_{16}$ revealed a deviation from a pure single Lorenz line in view of a possible significant contribution of dipole–dipole interactions between gadolinium ions (Fig. 18). The almost constant ΔB(T) dependence (Fig. 20) and an increase in *DI* with decrease in temperature (Fig. 21) indicate that the single domain particles with the fluctuating magnetization vector between the easy directions of magnetization do not interact. Below $T_B=30$ K in the superparamgnetic state, the magnetization vector is stable in the single domain and no interaction between domains is still observed.

The EPR spectra of $CoGd_4W_3O_{16}$ showed a single Lorenzian line in the temperature range of 10.2–188.5 K (Fig. 19). The line coming from the Co^{2+} ion, visible at 4.5 K, has clearly at least three components (see inset of Fig. 19) suggesting the Co^{2+} spin $S=3/2$. A simulation made at 5.6 K for Co^{2+} ($S=3/2$) with the aid of an EPR-NMR computer program [26] yields $\Delta B=23$ mT. The accordance with the experimental value is satisfactory. As a function of *T*, the EPR linewidth ΔB decreases to shallow minimum at 80 K. With further temperature reduction, the broadening of ΔB is observed; below the *DI* susceptibility characteristic temperature, $T_0=23$ K, ΔB increases rapidly (Fig. 21). At the same time, spin susceptibility *DI* increases and exhibits a sharp maximum at T_0, and below this temperature it rapidly decreases not reaching the zero value (Fig. 21), the opposite as found in the AFM $ZnCr_{2-x}In_xSe_4$ spinels with Néel temperature of 20 K [27]. It means that for $CoGd_4W_3O_{16}$, ordering temperature is far below 4.5 K. It is worth noting that temperature T_0 well correlates with the blocking temperature T_B. The observed behavior of the linewidth and double integration as well as the negative value of paramagnetic Curie–Weiss temperature (Table 1) for $CoGd_4W_3O_{16}$ is attributed to critical phenomena while approaching the AFM order. Weak intensity of the resonance spectrum at 4.5 K also indicates the AFM order. These results suggest that at T_0, a two-dimensional AFM correlation takes place between the planes consisting separately the single domain particles with Gd^{3+} and Co^{2+} ions.

3.3. Brillouin fit

Shapes of the magnetization isotherms and spontaneous magnetization as well as the magnetic hysteresis indicate that the majority of the (Co,Zn)$RE_4W_3O_{16}$ powder tungstates depicted in Figs. 8–15 show a superparamagnetic-like behavior. It is noteworthy that the widest hysteresis loop and saturation magnetization are observed for $ZnGd_4W_3O_{16}$ tungstate for which the Gd ions carry only a spin magnetic moment. On the other hand, superparamagnetism usually yields saturation curves with higher moments anyway. Nevertheless, the deviations from these features observed for the remaining tungstates may suggest a larger orbital contribution. It may particularly concern $ZnEu_4W_3O_{16}$ compound showing a strong red emission under 394 nm because for bulk europium metal this emission is absent. It is well known in literature [17,19,20] that narrower multiplet widths occur in the cases of europium and samarium, which are comparable to *kT*. Therefore, the effect of the electric charges associated with the surrounding ligands can lift the degeneracy of individual states, produced by the spin–orbit coupling, by an amount of the order of 100 cm^{-1}, which is not negligible [19]. Consequently, an electron transition of Eu^{3+} ion ($^7F_0 \rightarrow {}^5L_6$) in $ZnEu_4W_3O_{16}$ tungstate is observed [14].

In general, the hysteresis loop is observed in the powder tungstates under study below the blocking temperature of 30 K. In consequence, a structure containing small ferro- and/or ferrimagnetic single-domain particles may be formed, resulting in the powder samples enriched in (Co,Zn)$RE_4W_3O_{16}$ nanocrystalities with randomly oriented anisotropy fields. From the fundamental point of view, the hysteresis loop is not well understood, partly because of a complicated nature of the interactions among the particles in a cluster, although Luo et al. [28] showed that the peak in the curve of the ZFC temperature dependence of magnetization was due to interactions between the grains. As the temperature dependence of the ZFC susceptibility curves of the tungstates under study do not reveal any peak, one can conclude that no interactions between the grains exist.

In order to get estimates of the atomic moments containing orbital contribution in (Co,Zn)$RE_4W_3O_{16}$ tungstates, Brillouin procedure, which does not include any cluster interactions was used. Saturation magnetization at 4.2 K in paramagnetic region was reached almost for $ZnRE_4W_3O_{16}$ (where RE=Nd, Gd, Dy and Ho) and $CoRE_4W_3O_{16}$ (where RE=Sm, Eu and Gd) compounds. Their experimental virgin magnetization curves, σ(H/T), can be easily fitted by the following expression:

$$\sigma = \sigma_0 B_J(x) \tag{1}$$

where σ_0 is the magnetization at the highest value of *H/T*, $x=g_{fit}J\mu_B H/kT$, g_{fit} is the fitted Landé factor and the Brillouin function B_J is given by [17]

$$B_J(x) = \frac{2J+1}{2J}\coth\left(\frac{2J+1}{2J}\right)x - \frac{1}{2J}\coth\frac{x}{2J} \tag{2}$$

In case of $ZnRE_4W_3O_{16}$ tungstates, *J* in Eq. (2) is defined as an effective angular momentum. Since the experimental effective magnetic moment of these tungstates corresponds to the effective number of Bohr magnetons of the RE free ion, we assume as an effective angular momentum, angular momentum of the RE free ion. For Nd^{3+}, Gd^{3+}, Dy^{3+} and Ho^{3+} they are, respectively: 9/2, 7/2, 15/2 and 8. In case of $CoRE_4W_3O_{16}$ tungstates the experimental effective magnetic moment also correlate with the effective number of Bohr magnetons that is the vector sum of effective numbers of RE and Co ions (i.e., $p_{eff}=\sqrt{p_{Co}^2+4p_{RE}^2}$). So, according to the rule for angular momenta [29], the EPR results and the Brillouin procedure, *J* in Eq. (2) is defined as a sum of an effective angular momentum of RE ions and the effective spin of Co ones. The latter results from the fact that the *JLS*-coupling works for the protected RE 4*f*-shell, but not for the unprotected TM 3*d*-shell and only effective spin of 3/2 of Co ions for all the Co-based tungstates was assumed. The Brillouin procedure gave the best fitting when the agreement index R^2 reached maximum (Table 1) for $J=4$ ($CoSm_4W_3O_{16}$) and for $J=5$ ($CoGd_4W_3O_{16}$). The Brillouin functions for $ZnRE_4W_3O_{16}$ and

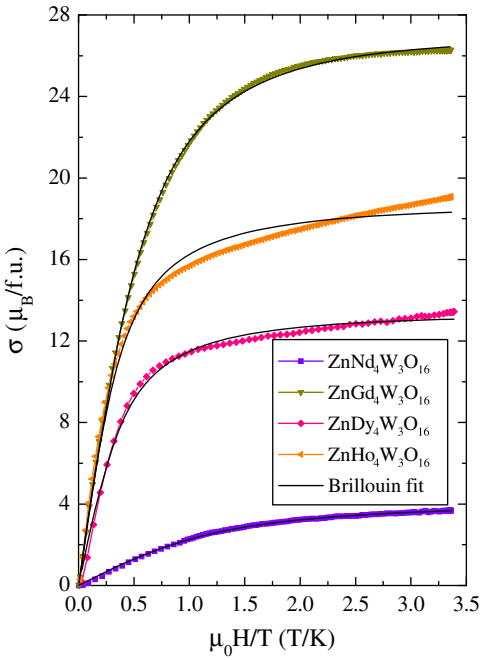

Fig. 22. σ vs. $\mu_0 H/T$ at 4.2 K for $ZnNd_4W_3O_{16}$ ($J=9/2$), $ZnGd_4W_3O_{16}$ ($J=7/2$), $ZnDy_4W_3O_{16}$ ($J=15/2$) and $ZnHo_4W_3O_{16}$ ($J=8$). The solid line is for a Brillouin curve fitted to the experimental data at the highest value of $\mu_0 H/T$.

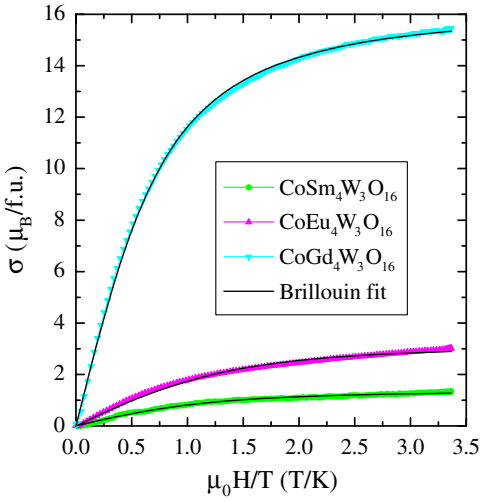

Fig. 23. σ vs. $\mu_0 H/T$ at 4.2 K for $CoSm_4W_3O_{16}$ ($J=4$), $CoEu_4W_3O_{16}$ ($J=3/2$) and $CoGd_4W_3O_{16}$ ($J=5$). The solid line is for a Brillouin curve fitted to the experimental data at the highest value of $\mu_0 H/T$.

$CoRE_4W_3O_{16}$ together with experimental data of magnetic moments are shown in Figs. 22 and 23, respectively. The accordance is satisfactory and these data are seen to fall on a universal Brillouin curve, indicating paramagnetic response [30]. The values of g_{fit} given in Table 1 are lower in comparison with the theoretical ones for free *RE*-ions of $ZnRE_4W_3O_{16}$, and they are generally closer to the *g*-factor value of Co^{2+} than the one for RE^{3+} in $CoRE_4W_3O_{16}$. It indicates that the stronger orbital contribution, the weaker the superparamagnetic effect. The opposite behavior for the spin contribution was observed.

4. Conclusions

We have measured dc and ac susceptibilities as well as the magnetization isotherms in the ZFC mode of powder (Co,Zn)$RE_4W_3O_{16}$ tungstates. Additionally, EPR measurements for $ZnGd_4W_3O_{16}$ and $CoGd_4W_3O_{16}$ were carried out. The results showed a paramagnetic state and a superparamagnetic-like behavior depending on strength of the spin–orbit coupling driven from the Brillouin fit of the Landé factor namely for $ZnRE_4W_3O_{16}$. The superparamagnetic particle saturation was also observed with their TM/RE tungstates. The hysteresis loops with zero remanence and coercivity as well as without a peak on the ZFC susceptibility curve indicate that the powder tungstates under study seem to be formed as the ferro- and/or ferrimagnetic single-domain particles not interacting with one another.

Acknowledgments

This work was partly supported by Ministry of Scientific Research and Information Technology (Poland) and funded from science resources for years 2009–2012 as a research project (Project No. N N209 336937). The authors are very grateful to Dr. P. Gusin and to Prof. D. Skrzypek from the Institute of Physics of the University of Silesia in Katowice for their helpful remarks.

References

[1] S. Neeraj, N. Kijima, A.K. Cheetham, Chem. Phys. Lett. 387 (2004) 2.
[2] T. Nishida, T. Ban, N. Kobayashi, Appl. Phys. Lett. 82 (2003) 3817.
[3] Q. Zeng, P. He, M. Pang, H. Liang, M. Gong, Q. Su, Solid State Commun. 149 (2009) 880.
[4] A.V. Zaushitsyn, V.V. Mikhailin, A.Yu. Romanenko, E.G. Khaikina, O.M. Basovich, V.A. Morozov, B.I. Lazoryak, Inorg. Mater 41 (2005) 766.
[5] T. Kim, S. Kang, J. Lumin. 122–123 (2007) 964.
[6] Ch.-H. Chiu, M.-F. Wang, Ch.-S. Lee, T.-M. Chen, J. Solid State Chem. 180 (2007) 619.
[7] T. Nakano, Y. Kawakami, K. Uematsu, T. Ishigaki, K. Toda, M. Sato, J. Lumin. 129 (2009) 1654.
[8] F.-S. Wen, X. Zhao, H. Huo, J.-S. Chen, E. Shu-Lin, J.-H. Zhang, Mater. Lett. 55 (2002) 152.
[9] Q. Dai, H. Song, X. Bai, G. Pan, S. Lu, T. Wang, X. Ren, H. Zhao, J. Phys. Chem. C 111 (2007) 7586.
[10] M. Thomas, P. Prabhakar Rao, M. Deepa, M.R. Chandran, P. Koshy, J. Solid State Chem. 182 (2009) 203.
[11] L.-Y. Zhou, J.S. Wei, F.Z. Gong, J.-L. Huang, L.-H. Yi, J. Solid State Chem. 181 (2008) 1337.
[12] M. Daturi, G. Busca, M.M. Borel, A. Leclaire, P. Piaggio, J. Phys. Chem. B 101 (1997) 4358.
[13] E. Tomaszewicz, Solid State Sci. 8 (2006) 508.
[14] E. Tomaszewicz, M. Guzik, J. Cybińska, J. Legendziewicz, Helv. Chim. Acta 92 (2009) 2274.
[15] E. Tomaszewicz, Thermochim. Acta 447 (2006) 69.
[16] A. Worsztynowicz, S.M. Kaczmarek, E. Tomaszewicz, Solid State Phenom. 128 (2007) 207.
[17] A.H. Morrish, Physical Principles of Magnetism, John Wiley & Sons, Inc., New York, 1965 (p. 47).
[18] T. Groń, E. Malicka, A.W. Pacyna, Physica B 404 (2009) 3554.
[19] A. Earnshaw, Introduction to Magnetochemistry, Academic Press, London, 1968 (p. 29).
[20] C. Kittel, Introduction to Solid State Physics, John Wiley & Sons, Inc., New York, 1960 (p. 218).
[21] P. Urbanowicz, E. Tomaszewicz, T. Groń, H. Duda, A.W. Pacyna, T. Mydlarz, Physica B 404 (2009) 2213.
[22] D.B. Brown, V.H. Crawford, J.W. Hall, W.E. Hatfield, J. Phys. Chem. 81 (1977) 1303.
[23] D. Nelson, W. ter Haar, Inorg. Chem. 32 (1993) 182.
[24] C.M. Hurd, Contemp. Phys. 23 (1982) 469.
[25] J.J. Prejean, M.J. Joliclerc, P. Mond, J. Phys. 41 (1980) 427.
[26] M.J. Mombourquette, J.A. Weil, D.G. McGavin, EPR-NMR User's Manual, Department of Chemistry, University of Saskatchewan, Saskatoon, SK, Canada, 1999.
[27] D. Skrzypek, E. Malicka, A. Waśkowska, A. Cichoń, J. Cryst. Growth 312 (2010) 471.
[28] W. Luo, S.R. Nagel, T.F. Rosenbaum, R.E. Rosensweig, Phys. Rev. Lett. 67 (1991) 2721.
[29] L.I. Schiff, Quantum Mechanics, McGraw-Hill Book Company, Inc., New York, 1955 (p. 148).
[30] S.A. Majetich, J.O. Artman, M.E. McHenry, N.T. Nuhfer, S.W. Stanley, Phys. Rev. B 48 (1993) 16845.